



Delineation of breast cancer cell hierarchy identifies the subset responsible for dormancy

SUBJECT AREAS:

DEVELOPMENTAL
BIOLOGY

CANCER MICROENVIRONMENT

CELL DIVISION

CELL GROWTH

Shyam A. Patel^{1,2}, Shakti H. Ramkissoon³, Margarette Bryan¹, Lillian F. Pliner¹, Gabriela Dontu⁴, Prem S. Patel⁵, Sohrab Amiri⁶, Sharon R. Pine⁶ & Pranela Rameshwar¹

¹Department of Medicine – Division of Hematology/Oncology, New Jersey Medical School, University of Medicine and Dentistry of New Jersey, Newark, NJ, USA, ²Graduate School of Biomedical Sciences, University of Medicine and Dentistry of New Jersey, Newark, NJ, USA, ³Department of Pathology, Brigham and Women's Hospital, Boston, MA, USA, ⁴Department of Research Oncology, King's College London School of Medicine, UK, ⁵Brookdale University Hospital, Brooklyn, NY, USA, ⁶Department of Medicine – Robert Wood Johnson Medical School and Cancer Institute of New Jersey, New Brunswick, NJ, USA.

Received
28 August 2012

Accepted
15 October 2012

Published
30 November 2012

Correspondence and
requests for materials
should be addressed to
P.R. (rameshwa@
umdj.edu)

The bone marrow (BM) is a major organ of breast cancer (BC) dormancy and a common source of BC resurgence. Gap junctional intercellular communication (GJIC) between BC cells (BCCs) and BM stroma facilitates dormancy. This study reports on a hierarchy of BCCs with the most immature subset ($Oct4^{hi}/CD44^{hi/med}/CD24^{-/+}$) demonstrating chemoresistance, dormancy, and stem cell properties: self-renewal, serial passaging ability, cycling quiescence, long doubling time, asymmetric division, high metastatic and invasive capability. *In vitro* and *in vivo* studies indicated that this subset was responsible for GJIC with BM stroma. Similar BCCs were detected in the blood of patients despite aggressive treatment and in a patient with a relatively large tumor but no lymph node involvement. In brief, these findings identified a novel BCC subset with stem cell properties, with preference for dormancy and in the circulation of patients. The findings establish a working cellular hierarchy of BCCs based on phenotype and functions.

The incidence of breast cancer (BC) remains relatively high, despite treatment advances¹. BC shows preference for metastasis to the bone marrow (BM)^{1,2}. In BM, the BC cells (BCCs) adapt cycling quiescence close to the endosteum by establishing gap junctional intercellular communication (GJIC) with stroma and by decreasing production of growth-promoting cytokines^{2,3}. GJIC are formed by connexins (Cxs), which when absent result in increased aggressiveness of BC^{4,5}. Elements of the hematopoietic-supporting stroma also form GJIC with each other⁶. This indicates that any drug that targets Cxs could be toxic to the hematopoietic system. In order to identify novel targets for dormant BCCs, it is imperative to first identify the BCC subset with preference for GJIC and then determine how the dormant phenotype is attained.

GJIC facilitates the passage of miRNA from stroma to BCCs, promoting quiescence⁷. This report addressed the hypothesis that an immature subset of BCCs, perhaps containing BC-initiating cells, is responsible for GJIC with stroma. BCC subsets were isolated, based on the expression of octamer-binding transcription factor 4 (*Oct4*)⁸. *Oct4* generates Oct4A and Oct4B. The latter produces three isoforms through an alternate translational start sites⁹. *Oct4* is expressed in cancer stem cells and is involved in chemoresistance, tumor survival and pluripotency^{10–16}. *Oct4* pseudogenes have been identified in solid tumors⁸.

BC stem cells were reported to be $CD44^{+}/CD24^{-}/Lin^{-}$, $ALDH1^{+}$, $CD133^{+}$, and characterized by the ability to efflux Hoechst dye^{17–20}. This study evaluated the functions of three different BCC subsets and then characterized each using specific and global gene expression and phenotype. The data established a working hierarchy of BCCs. Cells similar to those with an immature phenotype were found in the circulation of patients who were undergoing treatment and for triple-negative BC who have completed treatment. Here we report on BCCs with the highest *Oct4* expression ($Oct4^{hi}$) with preference for GJIC with stroma and resistance to carboplatin *in vivo*. Overall, these findings have important translational implications for drug resistance, dormancy and resurgence of BCCs and also provide a framework to develop an expanded hierarchy of BCCs.

Results

BCC subset with preference for GJIC. We reported on GJIC between BCCs and BM stroma for a dormant phenotype of BCCs⁷. Since not all of the BCCs successfully established GJIC with stroma we sought the identity of



the candidate subset. Three subsets were selected, based on the expression of GFP. The GFP gene was under the control of the *Oct4* regulatory region. We selected three subsets, $Oct4^{hi}$, $Oct4^{med}$ and $Oct4^{-}$ (Fig. 1A). *Oct4* expression is an indicator of pluripotent stem cells^{16,21}. GFP intensity was a surrogate of *Oct4* protein (Fig. 1B).

Since GJIC requires the expression of Cxs, we performed western blots for Cx26, Cx32 and Cx43. The band intensities were higher for Cx26 and Cx43 in $Oct4^{hi}$ BCCs (Figs. 1D/S1C). Cx32 was only detected in $Oct4^{hi}$ BCCs. The higher levels of Cxs in $Oct4^{hi}$ correlated with significantly ($p < 0.05$) higher frequency of GJIC with stroma

(Fig. S1D/bottom panels, Fig. 1E). Cx43 appeared to be increased in co-cultures of $Oct4^{hi}$ BCCs and stroma (Fig. S1D, top panel). The inhibitor of GJIC, 1-octanol, blunted the labeling for Cx43 (Fig. S1D, top).

The $Oct4^{hi}$ BCCs were highly invasive *in vitro* and *in vivo* (Figs. 1F/G; S4D). At 72 h after intravenous injection with 10^3 unsorted pEGFP1-*Oct3/4*-BCCs, *Oct4*-expressing BCCs were identified by labeling with PE-anti-cytokeratin (red). Yellow cells (GFP+ PE) were noted close to the endosteum, indicating the migration of $Oct4^{hi}$ BCCs (Fig. 1G). The $Oct4^{hi}$ BCCs in the endosteal region

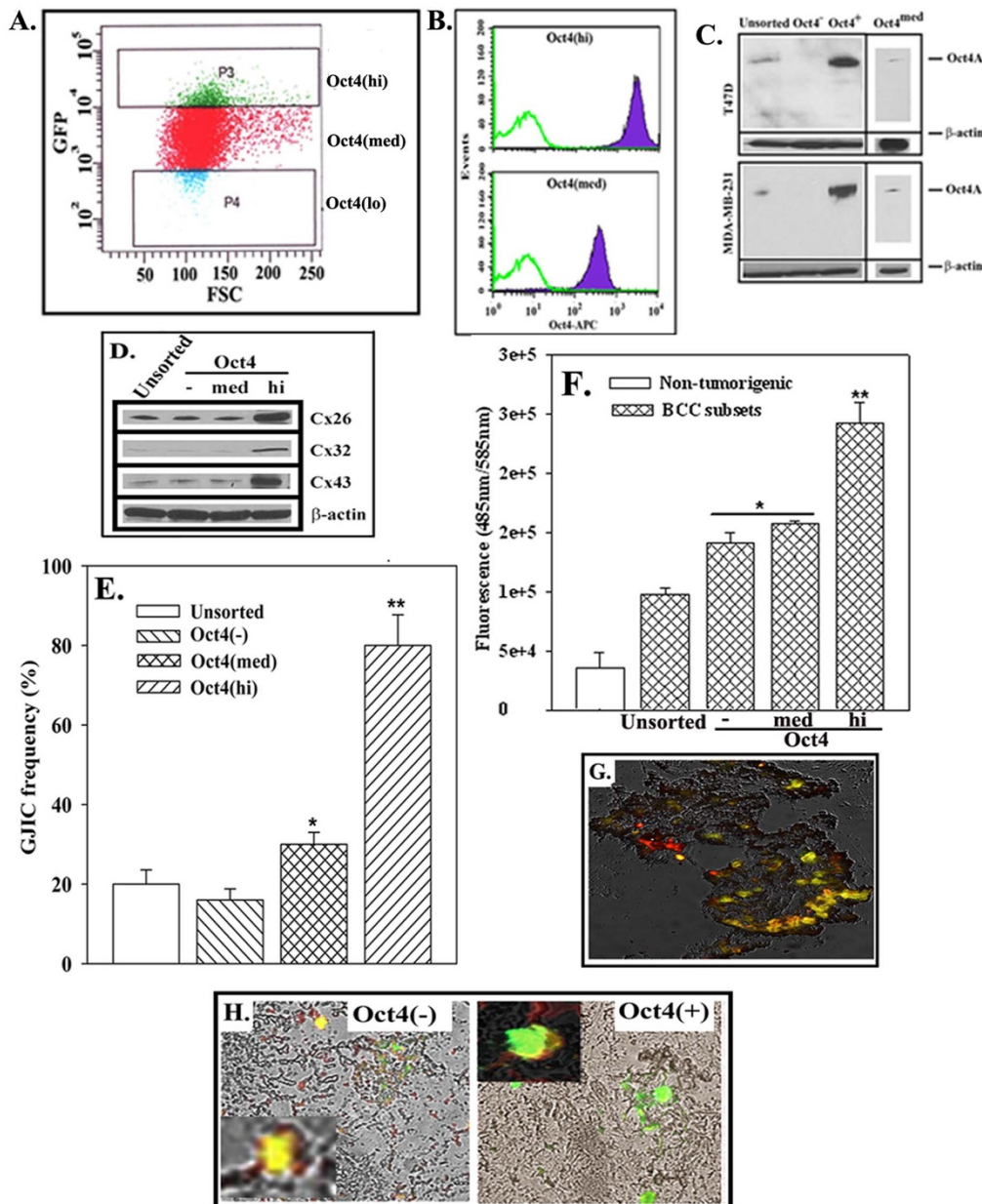


Figure 1 | GJIC by $Oct4^{hi}$ BCCs. A) Selection of BCC subsets with stable transfectants of pEGFP1-*Oct3/4*. The top and bottom 5% GFP intensities were designated $Oct4^{hi}$ and $Oct4^{low}$, respectively and the middle, $Oct4^{med}$. B) Intracellular flow cytometry for *Oct4* protein in $Oct4^{hi}$ and $Oct4^{med}$ subsets. C) Western blots for *Oct4* were performed with extracts from unsorted and sorted BCCs. The same blot is also shown for the *Oct4* component of Fig. 5E. D) Western blot ($n=4$) for Cxs with membrane extracts of BCC subsets. E) The frequency of GJIC with different BCC subsets are shown, mean \pm SD, $n=4$. F) Invasion of BCC subsets and non-tumorigenic MCF12A through matrigel, mean \pm SD, $n=4$. G) BALB/c mice were injected intravenously with 10^3 BCCs, stably transfected with pEGFP1-*Oct3/4*. After 72 h, the endosteal regions of femurs were examined microscopically (100x) for *Oct4* (+) BCCs by labeling with cytokeratin-PE⁺ (red). Yellow indicates the merging of PE (red) with GFP (green). H) CFDA-SE-labeled BCCs were injected intravenously and the cells close to the endosteum were labeled for cytokeratin-PE (red). Representative images are shown for $Oct4^{-}$ and $Oct4^{hi}$ BCCs (100x). ** $p < 0.05$ vs. other subset; * $p < 0.05$ vs. unsorted and $Oct4^{-}$ subset.



formed GJIC with endogenous BM cells. This was determined with CFDA-SE (green)-labeled BCCs. The green dye can be seen transferring to another cell, leaving the red-labeled cells. The red label was a result of PE-anti-cytokeratin (Fig. 1H, right panel). The Oct4⁻ BCCs retained the dye (yellow) (Fig. 1H, left panel).

Resistance of Oct4^{hi} BCCs to carboplatin. Oct4^{hi} subset showed preference for GJIC (Fig. 1E). We therefore studied the cells' sensitivity to carboplatin. First, we studied the change in tumor volume by injecting Oct4^{hi} BCC in the dorsal flank of nude BALB/c. When the tumors attained 0.5 cm³, the mice were injected with carboplatin intraperitoneally. Unsorted BCCs succumb to carboplatin at day 8 but Oct4^{hi} remained at ~0.2 cm³ (Fig. 2A). Next, we studied the Oct4^{hi} cells in the BM for sensitivity to carboplatin. Oct4^{hi} BCCs were injected intravenously and then treated with carboplatin at day 2 and 5. The GFP (bright) BCCs were retained close to the endosteum, indicating resistance to carboplatin (Fig. 2B).

Self-renewal of Oct4^{hi} BCCs, *in vitro*. This section reported on the self-renewal of Oct4^{hi} BCCs. First, we compared the three BCC subsets for tumorsphere formation and serial passaging. Oct4^{hi} BCCs formed a large tumorsphere as compared to Oct4^{med} BCCs (Fig. S2A). Limiting dilution and serial passaging indicated >96% efficient tumorsphere formation by Oct4^{hi} BCCs (Figs. 3A, S3A). Oct4^{med} BCCs failed to undergo serial passages.

Next, we examined the GFP intensities of the parental and daughter cells for Oct4^{hi} and Oct4^{med} BCCs. These studies would indicate

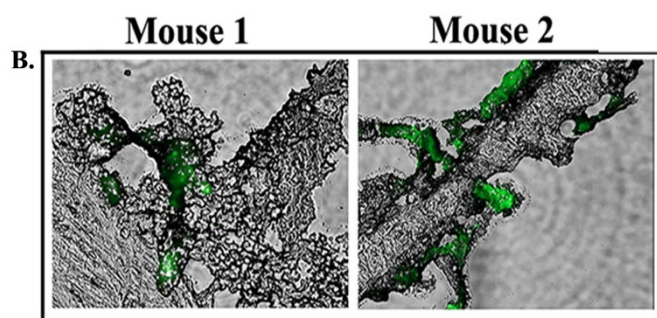
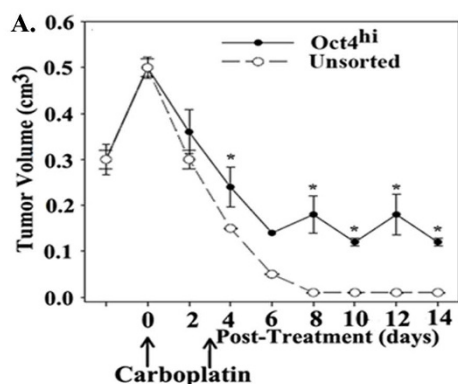


Figure 2 | Chemoresistance of Oct4^{hi} BCCs *in vivo*. A) Oct4^{hi} and unsorted BCCs were injected in the dorsal flank of nude BALB/c mice. When the tumor reached ~0.5 cm³ the mice were treated with carboplatin and the timeline changes in tumor volumes are measured. The data are presented as the mean tumor volume \pm SD, n = 10. * $p < 0.05$ vs. unsorted BCCs. B) Nude BALB/c mice (n = 10) were injected intravenously with 10³ unsorted pEGFP or pEGFP1-Oct3/4-transfected MDA-MB-231. After 24 h, the mice were injected intraperitoneally at 3-day intervals with carboplatin (50 mg/kg). After 1 wk, the endosteal regions were examined for GFP⁺ cells.

differences in self-renewal of the two subsets. The results showed similar intensities for the parental and daughter Oct4^{hi} BCCs (Figs. 3C, S3B), supporting self-renewal. Since the half life of Oct4 is ~20 h, the high GFP of the daughter Oct4^{hi} cell indicated constitutive expression of *Oct4*. In contrast, the GFP intensity of the daughter cell from Oct4^{med} BCCs was significantly lower than the parental (Figs. 3C, S3B).

If Oct4^{hi} BCCs are the most immature cell subset, they should be able to differentiate into heterogeneous subsets. We therefore placed freshly sorted Oct4^{hi} BCCs in culture for 2 wks and then studied the expanded cells for GFP intensity. Indeed, based on the mixed intensity, the results indicated heterogeneity (Fig. 3D). The low GFP intensity was not due to the loss of the vector or confounds of sorting (Figs. S2B/S2C). In order to validate that Oct4^{hi} BCCs can differentiate into different subsets, we used noble agar for colony size because the number of cell/colony is linked to the cell's maturity. Highly proliferating cells will form large colonies and slowly dividing cells are expected to form smaller colonies. We plated one Oct4^{hi} BCC in noble agar. At the first division, we selected the parental and daughter cells (Fig. S3B) and then expand in adherence cultures as for Fig. 3D. After 2 wks, the expanded cells were plated in noble agar. The resulted showed colonies with different number of cells (Figs. S3B/C). In summary, the *in vitro* studies supported self-renewal of Oct4^{hi} BCCs.

Serial passage of Oct4^{hi} BCCs, *in vivo*. The evidence of self-renewal by *in vitro* methods (Figs. 3A–D; S3B/C) were validated in serial passages, *in vivo*. Different numbers of Oct4^{hi} BCCs were injected in the dorsal flanks (P1) of nude BALB/c (n = 10). The time to attain 0.5 cm³ tumors was proportional to the number of injected cells (Fig. S4A). We harvested the tumors from the mice that were injected with 200 Oct4^{hi} BCCs and then selected the Oct4^{hi} cells for passage to naive mice. The process was repeated three times, totaling four passages (Fig. 3E). Unlike Oct4^{hi} BCCs that can be serially passaged, tumors from Oct4⁻ and Oct4^{med} BCCs regressed after 2 wks (Fig. S4B).

Division patterns of BCC subsets. The above studies supported Oct4^{hi} BCCs as functionally immature and with self-renewal ability. We therefore determined if there are differences in cell division and whether this can be supported at the molecular level. Proliferation studies indicated ~3-fold longer doubling time by Oct4^{hi} BCCs as compared to the other subsets (Fig. S5). This correlated with increases in G₁-linked p15 and p16 and decrease in G₁/S transition proteins (Cyclin D1 and Cdk 4) (Figs. 4A/S6A). In line with these findings, propidium iodide staining indicated >75% of Oct4^{hi} cells in G₀/G₁ phase (Fig. 4B).

We next performed time-lapse microscopy of representative bright-field and fluorescence images for Oct4⁺ (left) and Oct4⁻ (right) parental cells (green arrow), and the progenies of first, second and third divisions as orange, red and blue arrows, respectively (Fig. 4C). The first cell division for Oct4⁺ cell was 7 h and the cell cycle times of the daughter cells were 38 h and 64 h (Movie S1). The 38-h daughter cell divided into three cells with the death of one (yellow X) (Movie S1). The cell cycle rates of the daughters and granddaughters of Oct4⁻ were similar to each other (Fig. 4D, Movie S2): 2 h followed by 30 and 59 h (Movie S2). Asymmetric division of stem cells gave rise to daughters with different proliferative rates^{22,23}. Oct4⁺ cells showed a significantly longer cycling time as compared to Oct4⁻ cells (mean time = 32 h and 24 h, respectively, $p < 0.001$) (Fig. 4D). The cycling time of an Oct4⁺ cell varied from 24 to >68 h, whereas Oct4⁻ cell cycle times varied from 20 to 29 h, suggesting that Oct4⁺ cells give rise to daughters with different proliferative rates. Indeed, lineages of live images from multiple cell divisions over 68 h showed similar proliferative rates of Oct4⁻ progenies but marked differences in the proliferative rates of Oct4⁺ daughters (Figs. 4C/D). Asymmetric cell division was defined as a

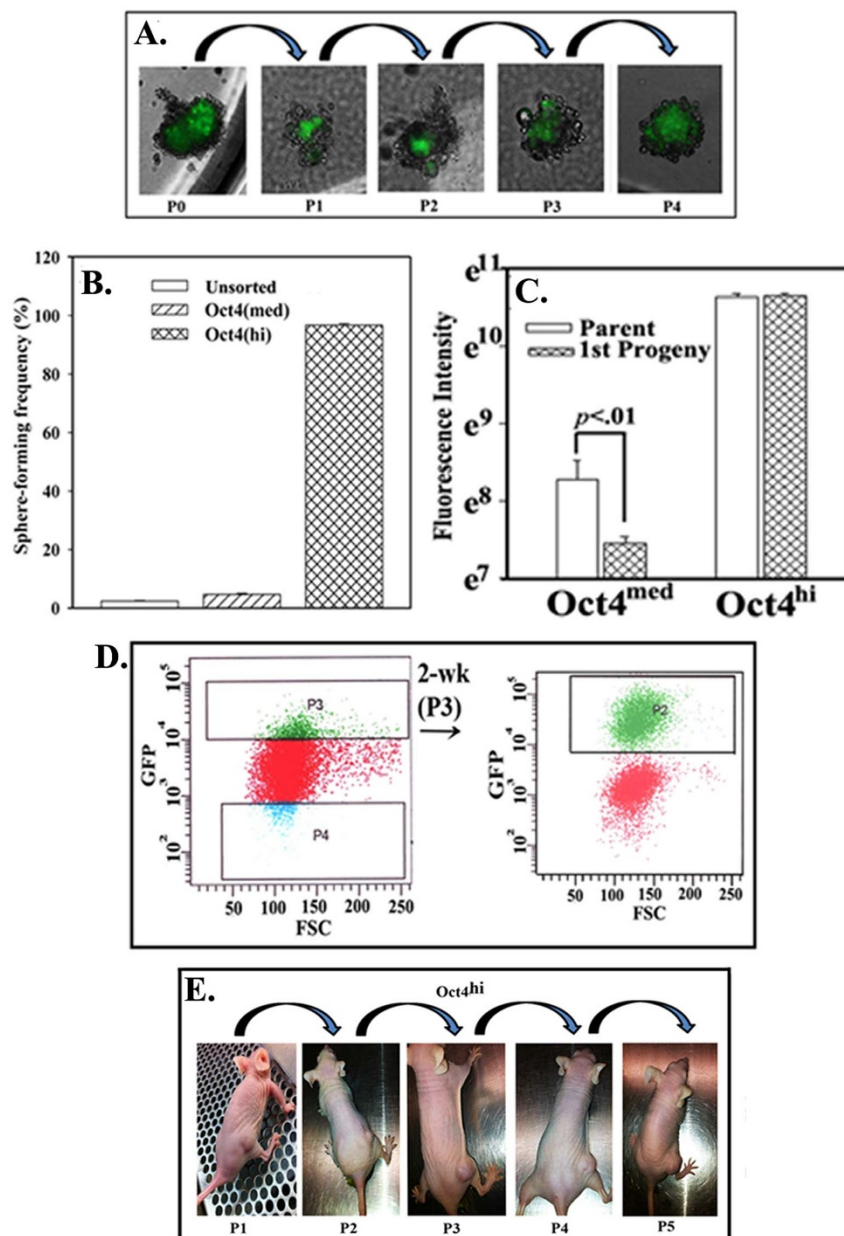


Figure 3 | Self-renewal of Oct4^{hi} BCCs. A) Serial passages of tumorsphere with 1 Oct4^{hi} cell. B) The frequencies (mean \pm SD, n=20) of tumorspheres are shown for unsorted, Oct4^{hi} and Oct4^{med} BCCs. C) The mean \pm SD (n=24) GFP intensities are shown for the parental and daughter of Oct4^{hi} and Oct4^{med} BCCs (Fig. S3B). D) Culture of freshly sorted Oct4^{hi} BCCs (left panel, also shown in Fig. 1A) for 2 wks resulted in a heterogeneous population, based on GFP expression (right panel). E) Serial passages of 200 Oct4^{hi} cells were performed in the dorsal flank of nude BALB/c.

difference in daughter cell cycle length of more than 8 h, or approximately 1/3 the doubling time of the first division. Over 47% of Oct4⁺ cells asymmetrically divided whereas none of the Oct4⁻ cells divided asymmetrically (Figs. 4E/4F). Of note, none of the several thousand Oct4⁻ cells monitored by time-lapse microscopy became Oct4⁺ cells (Movie S1), lending further credence to a hierarchical organization of BCC subsets under normal culture conditions.

Gene expression in BCC subsets. Functionally, the Oct4^{hi} BCCs appeared to be stem cells. We therefore analyzed the different subsets for the expression of genes linked to pluripotency. We also determined if there are differences in the expression of hormone receptor in the different subsets. Western blot and flow cytometry indicated high expressions of the drug resistant genes, MDR1 and ABCG2 (Figs. 4G, S6B). The blocker, verapamil, prevented 3-fold

exclusion of Hoechst dye in Oct4^{hi} BCCs as compared to no change for the other subsets (Figs. 4H/S7B).

We next examined a larger gene set with arrays and cDNA from Oct4^{hi/med} and Oct4⁻ cells (Figs. 5A/B). Ingenuity Pathway analyses with genes having >1.5-fold change in expression, showed a functional network consistent with pluripotency and cell cycle quiescence whereas those with <0.9-fold change in expression indicated cell proliferation (Figs. 5C/D). Together, these networks supported quiescence of Oct4-expressing cells. The array studies were expanded by western blot for stem cell-associated proteins. The results showed an increase in the expression of stem cell genes with extracts from Oct4^{hi} BCCs (Figs. 5E, S1A/B).

Intracellular flow cytometry were performed for estrogen receptor (ER) and progesterone receptor (PR). The resulted showed no change among the different subsets for the triple negative

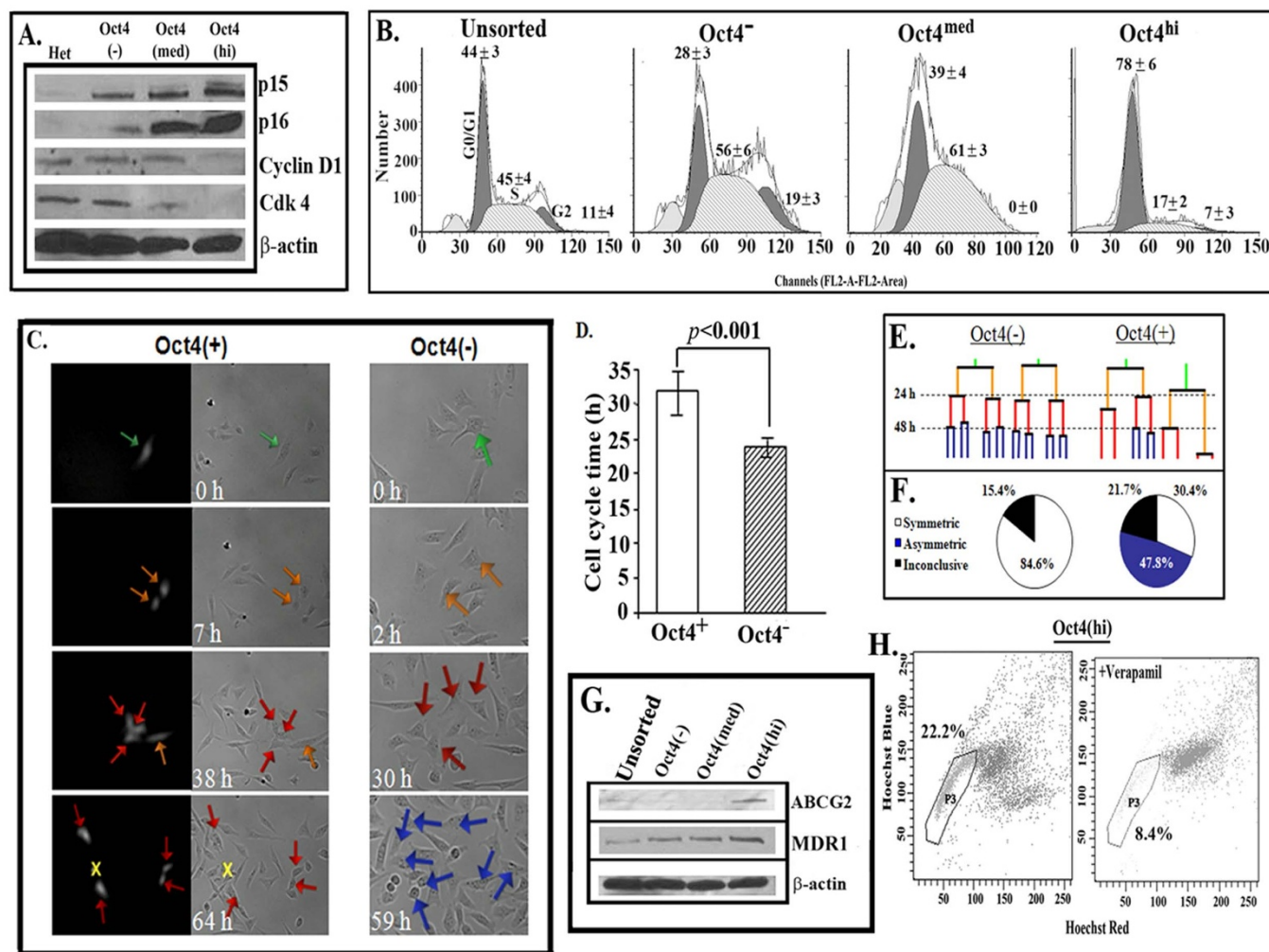


Figure 4 | Cycling and division patterns of BCC subsets. A) Western blots for cell cycle proteins were performed with nuclear extracts from unsorted and sorted BCCs. The data are shown for T47D. B) Analyses of cell cycle phase for BCC subsets by flow cytometry, using propidium iodide labeling. The data are shown for MDA-MB-231. C) Bright-field and fluorescence images of divided cells for an Oct4⁽⁺⁾ (left) and an Oct4⁽⁻⁾ (right) cell by video time-lapse microscopy. The parental cell is shown with a green arrow and progenies of first, second and third divisions, orange, red and blue arrows, respectively. The yellow X represents a non-viable cell. D) Oct4⁽⁺⁾ and Oct4⁽⁻⁾ BCCs were assessed for cell cycle time using time-lapse imaging; between anaphase of the parental and daughter cells. Data are presented as mean cell cycle \pm SD, $n = 50$ cells. E) An Oct4⁽⁺⁾ and Oct4⁽⁻⁾ cell and the progenies were tracked by time-lapse video microscopy for 68 h. The data are presented as lineages for the two subsets. The parental cells are shown as green vertical lines, and the progenies of the first, second and third cell divisions as orange, red, and blue, respectively. Vertical lines represent the time from 0 to 68 h, and dashed lines indicate 24 and 48 h after the start of real-time imaging. Oct4⁽⁻⁾ cells gave rise to daughters with similar proliferative rates whereas Oct4⁽⁺⁾ cells gave rise to both fast-dividing and slow-dividing daughters. F) The quantitative data of tracking multiple cell divisions from initial single cells over a 68 h time period show the relative frequency of asymmetric and symmetric cell divisions derived from single Oct4⁽⁺⁾ and Oct4⁽⁻⁾ cells. G) Western blots for ABCG2 and MDR1. H) Oct4^(hi) MDA-MB-231 and T47D were studied for the retention of Hoechst 33342 with or without verapamil. The analyses used Hoechst Blue and Red filters ($n = 5$). Marked subset shows dye efflux of the SP cells.

MDA-MB-231. However, in the triple positive T47D, heterogeneity was noted with respect to ER/PR expression. A small subset within the Oct4^(hi) T47D was determined to be ER⁽⁻⁾ (Fig. 5F).

Phenotype of BCCs - cell lines and primary tissues. Since we used Oct4 as a method to select subsets and there are multiple types of Oct4, we identified the Oct4 type in cell lines and primary BC tissues. Western blots with an antibody that detected all Oct4 types identified Oct4A (45 kDa) in BCCs and undetectable Oct4B and pseudogenes (Fig. 6A). A control for Oct4B used human mesenchymal stem cells and the results indicated predicted bands at 18, 21 and 29 kDa (Fig. 6A)¹⁰. The increase in Oct4 protein correlated with the respective mRNA (Figs. S8A/B). Immunohistochemical analyses indicated $\sim 1\%$ Oct4⁽⁺⁾ in BCC lines (Fig. S8C). Oct4 was detected in malignant and surrounding (Ctrl) breast tissues (Table S1;

Fig. 6B); with Oct4⁽⁺⁾ cells in the highly malignant areas of breast tissues (Fig. 6C). Oct4⁽⁺⁾/cytokeratin⁽⁺⁾ cells were identified in the blood of BC patients, including patients who were treated and who had negative lymph node status (Table S2; Fig. 6D). The presence of Oct4 could not be due to pseudogenes since only $\sim 14\%$ of cytokeratin⁽⁺⁾ cells from patients with BC were CD44⁽⁺⁾/CD24⁽⁻⁾ (Fig. 6E).

Phenotype of BCC subsets. CD44⁽⁺⁾/CD24^(-low)/lin⁽⁻⁾ have been reported as markers of BC stem cells^{17,24}. In order to analyze all the subsets for CD44 and CD24, we performed flow cytometry with 2-wk cultured Oct4^(hi) BCCs (Fig. 7A). The subset that we identified functionally as stem cells co-expressed CD24 (top/R3) with the upper 5%, CD24⁽⁺⁾ (middle/R3). The subset that we have identified as non-stem cells were mostly CD24⁽⁻⁾ (R2; lower/R3). We next analyzed the cells for CD44 in CD24⁽⁻⁾ BCCs (Fig. 7B)

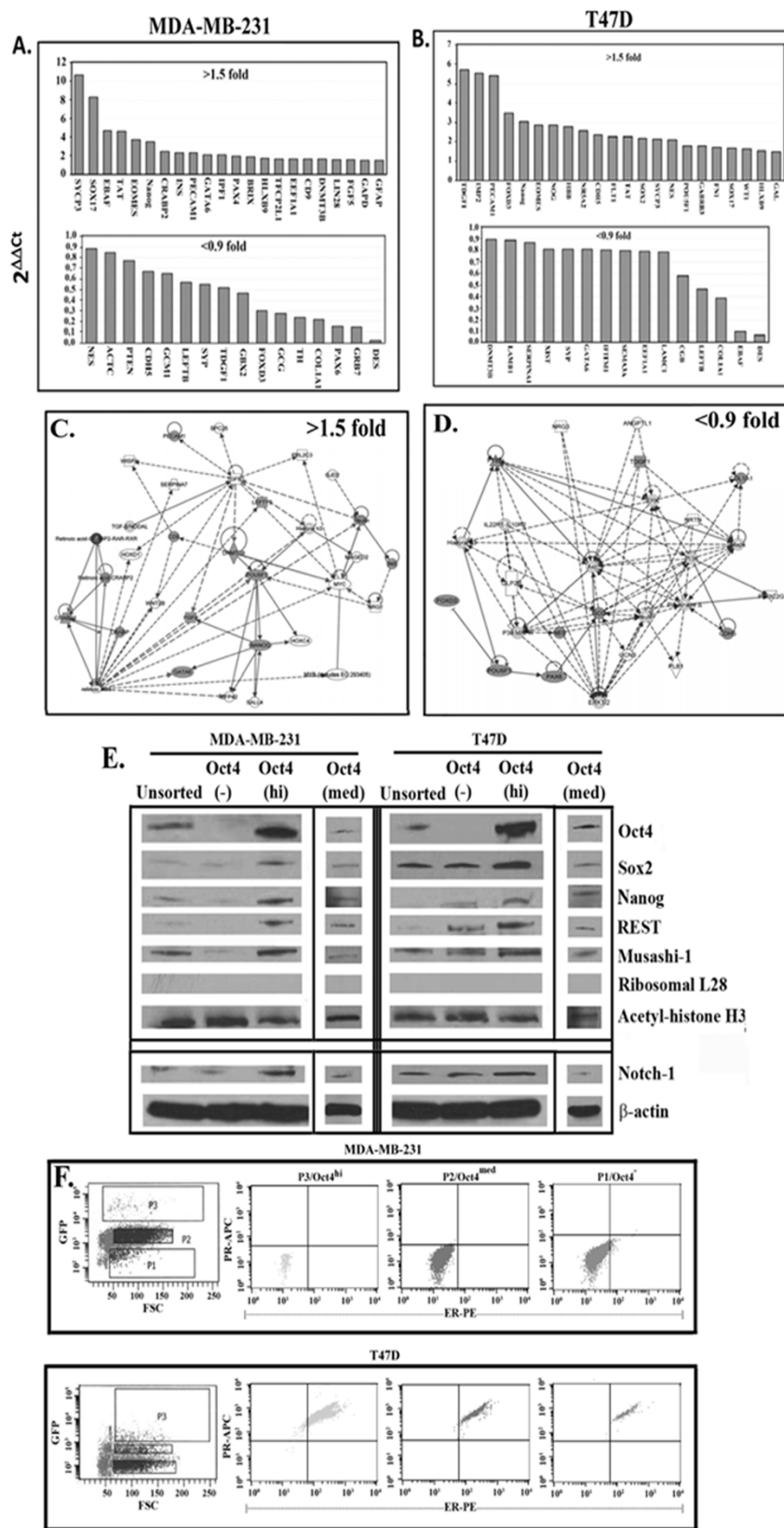


Figure 5 | Relative gene expressions in BCC subsets. A & B Taqman Stem Cell Array compared gene expression in Oct4⁺ and Oct4⁻ MDA-MB-231 (A) and T47D (B). C & D The output values were normalized to the internal control and then presented as $\Delta\Delta Ct$ of Oct4^{hi}/Oct4⁻. The genes showing >1.5 (C) and <0.9 fold (D) differences were analyzed with Ingenuity Pathway Program. E) BCC subsets were studied for stem cell-associated proteins by western blots with nuclear extracts. Notch-1 was analyzed with cytoplasmic extracts. Blots for acetyl-histone H3 and ribosomal protein L28 verified the purity of the compartmentalized extracts. F) Flow cytometry was performed for progesterone (PR) and estrogen (ER) receptors in BCC subsets.

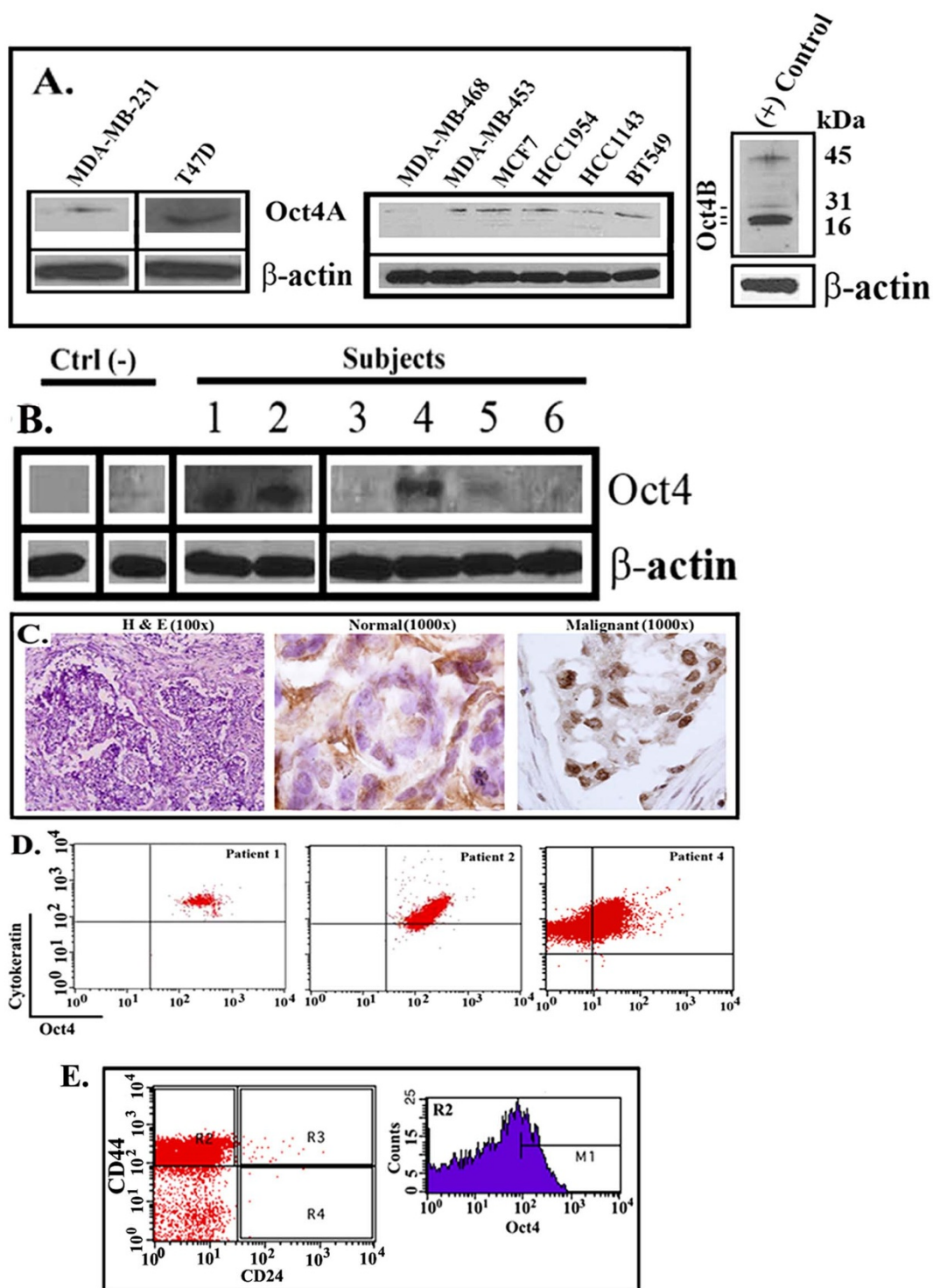


Figure 6 | *Oct4* expression in BCCs. **A & B** Western blots were performed with whole cell extracts from BCC lines (**A**) and primary breast tissues: malignant and surrounding (Ctrl) areas (**B**). The antibody detected all isoforms of *Oct4*, as shown in the right panel (**A**). **C** Immunohistochemistry with malignant and surrounding normal tissues (Table S1) were stained with hematoxylin and eosin (H&E) (100x) or labeled with anti-*Oct4*, diaminobenzidine (DAB) and HRP (1000x). **D** Flow cytometry with peripheral blood mononuclear cells from BC patients for cytokeratin (PE) and *Oct4* (FITC). Shown are the cells within the threshold of PE emission (cytokeratin+) that co-expressed *Oct4*. The analyses represent 9 subjects (Table S2). **E** Cytokeratin(+) cells in the blood of three patients (one Stage 1 and two Stage 3) were analyzed for CD44 and CD24 and the CD44⁺/CD24⁻ cells (R2) were further studied for *Oct4*.

and the results indicated heterogeneity in CD44 expression within *Oct4*^{hi} and *Oct4*^{med} BCCs. The results also showed a subset that was CD44^{dim}/*Oct4*^{hi} (lower box). *Oct4*^{hi}/CD24⁺ BCCs (~4%,

Fig. 7A; middle/R3) were further analyzed, based on cell size (Fig. 7C, left) and the results showed CD24⁺ cells within the larger subset (R3; right). The phenotypic data were combined

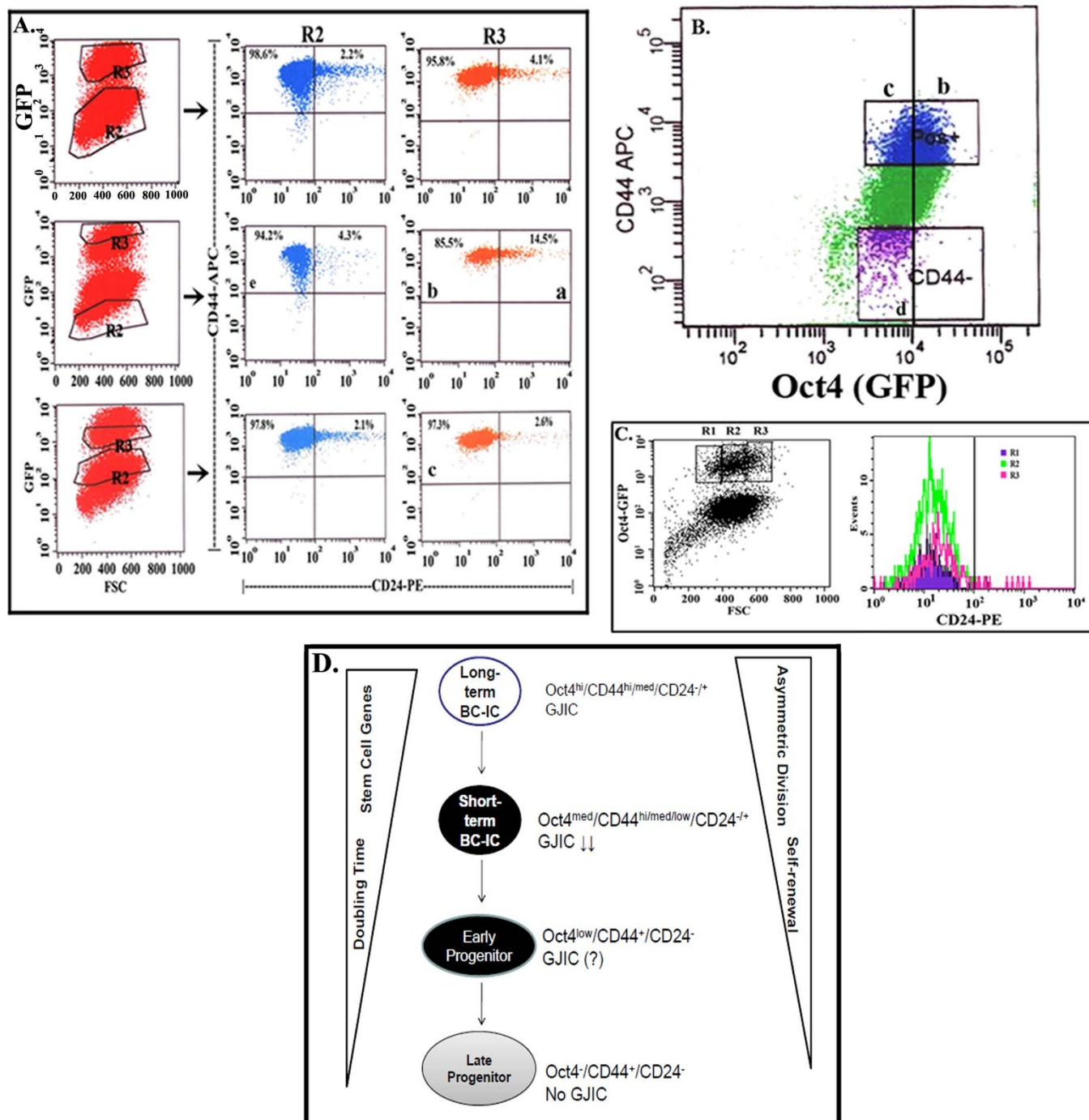


Figure 7 | Phenotypic analyses of BCCs and hierarchical representation of BCC subsets. A) pEGFP1-Oct3/4-transfectants were analyzed for CD44 and CD24 by flow cytometry. B) CD24⁺ cells were depleted from pEGFP1-Oct3/4- transfectants and then analyzed for CD44 and Oct4 (GFP). C) The top GFP⁺ cells (Oct4^{hi}) were further analyzed, based on size (R1–R3), for CD24. D) A working hierarchy, based on function and phenotype.

with the functional studies to develop a working hierarchy (Fig. 7D).

Similarity of BCCs in nude mice. This set of studies determined if the phenotype of the GFP-selected BCCs were retained *in vivo*. Oct4^{hi} BCCs, *in vitro*, differentiate in a mixed subset within two weeks (Fig. 3D). We therefore asked if this self-renewal/differentiation occurs *in vivo*. We selected passage 3 tumors (Fig. 3E) and then analyzed the suspended cells for Oct4 expression by flow cytometry. The results showed a mixed subset (Fig. 3A, top right and lower panels).

Since we found all subsets of the BCCs expressing CD44, we determined if the same occurred when the BCCs were *in vivo*. We therefore injected Oct4⁻ (Fig. S4) and Oct4^{hi} BCCs (Fig. 3E) and after one and two weeks, respectively, we studied the tumors for CD44 expression. In both cases, CD44 was retained in the tumors (Fig. 8B). We next studied the BCCs in the femurs of mice for Oct4 expression, based on GFP. Mice that were injected intravenously with Oct4⁻ and Oct4⁺ BCCs. After 5 days, cytokeratin cells were selected and then studied for GFP expression by flow cytometry. Those injected with the former continued to be GFP(-) (Fig. 8C) whereas those injected with Oct4⁺ BCCs expressed GFP (Fig. 8D). In

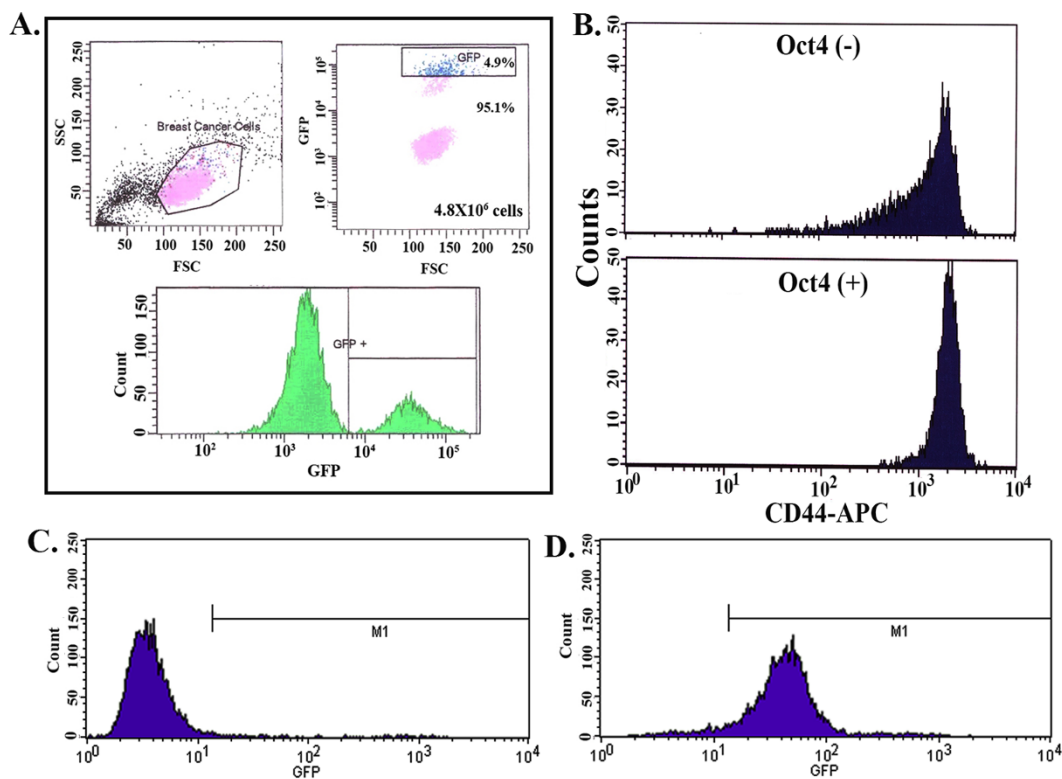


Figure 8 | Phenotype of *in vivo* BCC subsets. A) Suspension cells from passage 3 tumors in nude mice were analyzed by flow cytometry for subsets, based on GFP expression. B) Nude BALB/c injected with Oct4^{hi} and Oct4⁻ BCCs subcutaneously. The cells were CD44⁺ as shown in Fig. 7B. After one (Oct4⁻) and two (Oct4^{hi}) weeks, the tumors were removed and then reanalyzed for CD44 expression by flow cytometry. C & D) Nude BALB/c mice were injected intravenously with Oct4⁻ (C) and Oct4⁺ (D) BCCs. After five days, cytokeratin(+) cells were selected in the femurs and then studied for Oct4 expression.

summary, the cells selected based on GFP retained the same properties *in vivo*.

Discussion

The identity of BC stem cells remains a subject of investigation. Regardless of the phenotype, it is accepted that BC stem cells express genes linked to pluripotency^{25,26}. Among the BCC subsets studied, only Oct4^{hi} cells initiated tumors without evidence of regression, showed self-renewal property, expressed stem cell genes and divided asymmetrically. Oct4 is expressed at low frequency in BCC lines, and in cellular clusters within the malignant areas of breast tissues (Fig. 6). Regardless of treatment with chemotherapy, Oct4⁺/cytokeratin⁺ cells were detected in the blood of BC patients, indicating their resistance to chemotherapy (Fig. 6). We identified Oct4⁺/cytokeratin⁺ BCCs in the blood of patients, even when the lymph nodes were negative for BCCs. Although further studies are required, these pilot studies, together with the other findings in this report, suggested that the most immature BCCs may bypass the lymph nodes. In line with these observations, the Oct4^{hi} BCCs have been shown to rapidly enter the lungs and brain of mice (Fig. S4D). These findings are consistent with the ongoing debate on the benefit of dissecting lymph nodes in BC patients²⁷.

The Oct4^{hi} BCCs from cell lines appear to be similar to the cells found in patients (Fig. 6). After the final treatment of patients with triple negative BCCs, the cells in blood were Oct4(+). The similarity of the selected cells with those *in vivo* (Fig. 8) indicated that the surviving cells in BM, close to the endosteum forming GJIC with endogenous cells (Figs. 1 and 6), could be similar to the resistant BCCs in patients. BCCs show preference for BM where they can resurge after prolong remission for tertiary metastasis with poor outcome^{28,29}. The property of the BCCs in BM has not been studied. Our findings suggest that the cells that form GJIC and have tumor-initiating properties could be similar to our selected cells.

Tumor-initiating Oct4^{hi} BCCs resisted carboplatin and are efficient in establishing GJIC with stroma close to the endosteum (Fig. 1). These findings underscore the significance to BC dormancy and drug resistance. It is unclear if the cycling quiescence of Oct4^{hi} BCCs caused the cells' resistance to carboplatin, which requires rapidly dividing cells for effectiveness³⁰. Other studies have similarly reported on selective chemoresistance by cancer stem cells^{31,32}. The studies in this report will allow us to expand on our previous findings in which we observed the passage of miRNAs through GJIC, a process that facilitates BCC quiescence in BM³³. The chemoresistance of Oct4^{hi} BCCs should be taken in the context of the other findings, such as circulating Oct4(+) BCCs in patients and preference for GJIC with stroma. Our studies might provide answers to explain why the BM might be a nidus for cancer resurgence after years of remission²⁷ as well as a source of BCC protection³⁴. The chemoresistance shown in the *in vivo* studies and chemosensitivity by the Oct4^{lo/-} BCCs are supported by the informatics studies with regards to cell proliferation and quiescence (Fig. 5).

CD44/CD24 has been widely used to isolate BC stem cells^{17,35,36}. In our studies, CD44 and CD24 can demarcate cells within the hierarchy, which was established based on function, phenotype and gene expression (Fig. 7). Side population (SP) cells can resist chemotherapy and has been shown to contain the cancer stem cells^{37,38}. In our studies, not all Oct4^{hi} cells effluxed the Hoechst dye and expressed ABCG2 (Figs. 4/S7), suggesting that stem cells might be present in the non-SP subsets. Precedent for this has been reported for glioma cells³⁹. ABCG2 does not always correlate with SP since there are 30 proteins within the family.

In summary, we have developed a hierarchy of BCCs, based on function, phenotype and gene expression. The hierarchy forms the impetus for further subdivision based on cell maturity. The expansion of the hierarchy will allow studies on dedifferentiation and to evaluate how BCCs can be efficiently targeted with reduced toxicity. The cells with the least maturity could self-renew and



undergo serial passages, *in vivo*. More importantly, we have identified the subset of BCCs that shows functional GJIC with BM stroma and explains dormancy and chemoresistance.

Methods

Isolation of BCC subsets. MDA-MB-231 and T47D were stably transfected with pEGFP1-Oct3/4, which expresses green fluorescent protein (GFP) under the control of Oct4 promoter. pEGFP1-Oct3/4 was generously provided by Dr. Wei Cui (Imperial College London, UK)⁴⁰. Stable transfectants were obtained with 600 and 400 $\mu\text{g}/\text{ml}$ of G418 for MDA-MB-231 and T47D, respectively. Immediately before the assays, subsets were sorted using the FACSDiva (BD Biosciences), based on the intensity of GFP of singlets. The top 5% was designated Oct4^{hi} and the lower 5%, Oct4⁺. Those between the two extremes were designated Oct4^{med}.

Human subjects. The use of human tissues was approved by the Institutional Review Board of the UMDNJ-Newark Campus and Brookdale University Hospital. Stromal cells were cultured from BM aspirates. Surgical tissues from malignant and normal areas of the breast were obtained from Brookdale University Hospital, NY (Table S1). Peripheral blood was obtained from patients with BC (Table S2).

Tumorsphere assay and *in vitro* serial passage. BCCs were seeded at 1/well in serum-free media in 96-well low-adhesion plates (Costar, Corning, NY). At day 10, a positive tumorsphere contained >20 cells. One tumorsphere was dissociated with trypsin and then mechanically with a syringe and a 27 gauge needle. The cells were passed through a 40 μm mesh (BD cell strainer cap tube) and then resorted for limiting dilutions at 1 cell/well. This process was repeated 5 times.

Array analyses. Gene expression analyses were performed with Taqman Stem Cell Pluripotency Array (Applied Biosystem), by quantitative RT-PCR, using ABI 7900. The fold change between subsets were calculated using the $\Delta\Delta\text{Ct}$ method as follows: $(\text{Ct}_{\text{Oct4}(\text{hi})} - \text{Ct}_{\text{Gene of Reference}}) / (\text{Ct}_{\text{Oct4}(\text{+})} - \text{Ct}_{\text{Gene of Reference}})$.

The fold changes were entered into Ingenuity Pathway Analysis (Ingenuity[®] Systems, www.ingenuity.com) for pathway networks, as described⁷. The analyses allowed for the identification of complex biological interactions based on at least one published reference in the database. Biological predictions were made based on protein-protein interactions, and the insights into molecular pathways were gathered.

Time-lapse microscopy. Time-lapse microscopy of MDA-MB-231 cells was performed with Axiovert 200 M fluorescence microscope (Carl Zeiss, Inc.) at constant conditions of 37°C and 5% CO₂. Brightfield and fluorescence images were acquired every 10 min for up to 68 h using a 10x objective (Zeiss) and an AxioCam MRm camera with Axiovision software v4.6 (Zeiss). Individual images were adjusted for brightness using the Axiovision software and exported to ImageJ (National Institutes of Health, Bethesda, MD), where the movies were assembled. Individual cells were tracked manually.

***In vivo* studies.** Female athymic BALB/c mice (4 wks) were obtained from Harlan Laboratories (Somerville, NJ) and housed in a laminar flow hood at an AAALAC-accredited facility. The use of mice was approved by the Institutional Animal Care and Use Committee, New Jersey Medical School (Newark, NJ).

Serial passages were performed by injecting different numbers of BCCs in the dorsal flanks of mice. The cells were resuspended in PBS and matrigel at 1:1 ratio in 0.2 mL volume. Tumors were monitored daily for 30 days and measured in two dimensions with a caliper. Tumor volume (V) was calculated as follows: $V = \pi r^2 h$, where r = radius and h = height. Subsequent passages occurred by sorting the initial subset and then repeating the injections.

***In vivo* migration** of BCCs to the BM of nude mice was studied by intravenously injecting 10³ pEGFP1-Oct3/4 stable transfectants. After 72 h, the femurs were flushed to eliminate the cells within the central region. After this, femurs were transected longitudinally and the endosteal cells were acquired by scraping with a blunt spatula. Cells were then labeled by immunocytochemistry for cytokeratin, as described above.

GJIC was assessed by dye transfer from BCCs to stroma in nude BALB/c and was investigated by injecting CFDA-SE-labeled Oct4^{hi} BCCs intravenously. After 72 h, the endosteal region cells were collected as above and then labeled for cytokeratin.

Carboplatin responses to tumor growth were assessed by subcutaneous injection of 200 Oct4^{hi} BCCs in matrigel in the dorsal flank. For unsorted BCCs, 10⁶ cells were injected. At ~0.5 cm³ tumors, mice were injected with carboplatin (50 mg/kg), twice, at 3-day intervals. Tumor sizes were recorded every 2 days with a caliper, as described for serial passage.

Statistical analyses. Data were analyzed using 2-tailed Student's t-test, analysis of variance and Tukey-Kramer multiple comparisons test. A p value less than or equal to 0.05 was considered significant.

- Kakarala, M. & Wicha, M. S. Implications of the cancer stem-cell hypothesis for breast cancer prevention and therapy. *J Clin Oncol* **26**, 2813–2820 (2008).
- Corcoran, K. E. *et al.* Mesenchymal stem cells in early entry of breast cancer into bone marrow. *PLoS One* **3**, e2563 (2008).

- Rao, G. *et al.* Facilitating Role of Preprotachykinin-I Gene in the Integration of Breast Cancer Cells within the Stromal Compartment of the Bone Marrow. *Cancer Res* **64**, 2874–2881 (2004).
- Bodenstine, T. M. *et al.* Homotypic Gap Junctional Communication Associated with Metastasis Suppression Increases with PKA Activity and Is Unaffected by PI3K Inhibition. *Cancer Res* **70**, 10002–10011 (2010).
- King, T. J., Fukushima, L. H., Yasui, Y., Lampe, P. D. & Bertram, J. S. Inducible expression of the gap junction protein connexin43 decreases the neoplastic potential of HT-1080 human fibrosarcoma cells *in vitro* and *in vivo*. *Mol Carcinog* **35**, 29–41 (2002).
- Milsom, M. D. & Trumpp, A. Bridging the information gap. *Nat Immunol* **12**, 377–379 (2011).
- Lim, P. K. *et al.* Gap Junction-Mediated Import of MicroRNA from Bone Marrow Stromal Cells Can Elicit Cell Cycle Quiescence in Breast Cancer Cells. *Cancer Res* **71**, 1550–1560 (2011).
- Liedtke, S., Stephan, M. & Kogler, G. Oct4 expression revisited: potential pitfalls for data misinterpretation in stem cell research. *Biol Chem* **389**, 845–850 (2008).
- Zhang, W. *et al.* Mapping of the minimal internal ribosome entry site element in the human embryonic stem cell gene OCT4B mRNA. *Biochem Biophys Res Commun* **394**, 750–754 (2010).
- Wang, X. & Dai, J. Concise Review: Isoforms of OCT4 Contribute to the Confusing Diversity in Stem Cell Biology. *Stem Cells* **28**, 885–893 (2010).
- Wang, X. Q. *et al.* Octamer 4 (Oct4) mediates chemotherapeutic drug resistance in liver cancer cells through a potential Oct4-AKT-ATP-binding cassette G2 pathway. *Hepatology* **52**, 528–539 (2010).
- Levings, P. P. *et al.* Expression of an Exogenous Human Oct-4 Promoter Identifies Tumor-Initiating Cells in Osteosarcoma. *Cancer Res* **69**, 5648–5655 (2009).
- Linn, D. E. *et al.* A Role for OCT4 in Tumor Initiation of Drug-Resistant Prostate Cancer Cells. *Genes Cancer* **1**, 908–916 (2010).
- Beltran, A. *et al.* Generation of tumor-initiating cells by exogenous delivery of OCT4 transcription factor. *Breast Cancer Res* **13**, R94 (2011).
- Kim, R. J. & Nam, J. S. OCT4 Expression Enhances Features of Cancer Stem Cells in a Mouse Model of Breast Cancer. *Lab Anim Res* **27**, 147–152 (2011).
- Tsai, C. C., Su, P. F., Huang, Y. F., Yew, T. L. & Hung, S. C. Oct4 and Nanog Directly Regulate Dnmt1 to Maintain Self-Renewal and Undifferentiated State in Mesenchymal Stem Cells. *Mol Cell* **47**, 169–182 (2012).
- Al-Hajj, M., Wicha, M. S., Ito-Hernandez, A., Morrison, S. J. & Clarke, M. F. Prospective identification of tumorigenic breast cancer cells. *Proc Natl Acad Sci* **100**, 3983–3988 (2003).
- Ginestier, C. *et al.* ALDH1 Is a Marker of Normal and Malignant Human Mammary Stem Cells and a Predictor of Poor Clinical Outcome. *Cell Stem Cell* **1**, 555–567 (2007).
- Liu, S. & Wicha, M. S. Targeting Breast Cancer Stem Cells. *J Clin Oncol* **28**, 4006–4012 (2010).
- Wright, M. *et al.* Brca1 breast tumors contain distinct CD44+/CD24- and CD133+ cells with cancer stem cell characteristics. *Breast Cancer Res* **10**, R10 (2008).
- Greco, S. J., Liu, K. & Rameshwar, P. Functional Similarities Among Genes Regulated by Oct4 in Human Mesenchymal and Embryonic Stem Cells. *Stem Cells* **25**, 3143–3154 (2007).
- Cicalese, A. *et al.* The Tumor Suppressor p53 Regulates Polarity of Self-Renewing Divisions in Mammary Stem Cells. *Cell* **138**, 1083–1095 (2009).
- Costa, M. R. *et al.* Continuous live imaging of adult neural stem cell division and lineage progression *in vitro*. *Development* **138**, 1057–1068 (2011).
- Clarke, M. F. *et al.* Cancer Stem Cells—Perspectives on Current Status and Future Directions: AACR Workshop on Cancer Stem Cells. *Cancer Res* **66**, 9339–9344 (2006).
- Hu, T. *et al.* Octamer 4 small interfering RNA results in cancer stem cell-like cell apoptosis. *Cancer Res* **68**, 6533–6540 (2008).
- Lengerke, C. *et al.* Expression of the embryonic stem cell marker SOX2 in early-stage breast carcinoma. *BMC Cancer* **11**, 42 (2011).
- Giuliano, A. E. *et al.* Axillary Dissection vs No Axillary Dissection in Women With Invasive Breast Cancer and Sentinel Node Metastasis. *JAMA: J Am Med Assoc* **305**, 569–575 (2011).
- Alix-Panabieres, C., Riethdorf, S. & Pantel, K. Circulating Tumor Cells and Bone Marrow Micrometastasis. *Clin Cancer Res* **14**, 5013–5021 (2008).
- Wiedswang, G. *et al.* Isolated Tumor Cells in Bone Marrow Three Years after Diagnosis in Disease-Free Breast Cancer Patients Predict Unfavorable Clinical Outcome. *Clin Cancer Res* **10**, 5342–5348 (2004).
- McKnight, J. A. Principles of chemotherapy. *Clin Tech Small Anim Pract* **18**, 67–72 (2003).
- Calcagno, A. M. *et al.* Prolonged drug selection of breast cancer cells and enrichment of cancer stem cell characteristics. *J Natl Cancer Inst* **102**, 1637–1652 (2010).
- Honoki, K. *et al.* Possible involvement of stem-like populations with elevated ALDH1 in sarcomas for chemotherapeutic drug resistance. *Oncol Rep* **24**, 501–505 (2010).
- Pantel, K. & Ott, M. Occult micrometastasis: enrichment, identification and characterization of single disseminated tumour cells. *Sem Cancer Biol* **11**, 327–337 (2001).



34. Patel, S. A. *et al.* Mesenchymal stem cells protect breast cancer cells through regulatory T cells: role of mesenchymal stem cell-derived TGF-beta. *J Immunol* **184**, 5885–5894 (2010).
35. Cirenajwis, H. *et al.* Reduction of the putative CD44+. *Anticancer Drugs* **21**, 897–906 (2010).
36. Wang, K. H. *et al.* Increasing CD44+/CD24(–) tumor stem cells, and upregulation of COX-2 and HDAC6, as major functions of HER2 in breast tumorigenesis. *Mol Cancer* **9**, 288 (2010).
37. Hiraga, T., Ito, S. & Nakamura, H. Side population in MDA-MB-231 human breast cancer cells exhibits cancer stem cell-like properties without higher bone-metastatic potential. *Oncol Rep* **25**, 289–296 (2011).
38. Kobayashi, Y. *et al.* Side population is increased in paclitaxel-resistant ovarian cancer cell lines regardless of resistance to cisplatin. *Gynecol Oncol* **121**, 390–394 (2011).
39. Broadley, K. W. *et al.* Side Population is not Necessary or Sufficient for a Cancer Stem Cell Phenotype in Glioblastoma Multiforme. *Stem Cells* **29**, 452–461 (2010).
40. Gerrard, L., Zhao, D., Clark, A. J. & Cui, W. Stably transfected human embryonic stem cell clones express OCT4-specific green fluorescent protein and maintain self-renewal and pluripotency. *Stem Cells* **23**, 124–133 (2005).

Acknowledgements

Grant Support: Department of Defense (W81XWH-10-1-0413). This work was done at UMDNJ-New Jersey Medical School, Department of Medicine, Newark, NJ 07103. This work is in partial fulfillment for a Ph.D. degree to Shyam A. Patel.

Author contributions

SAP designed and conducted 90% of the studies; SHR conducted the immunohistochemistry; PSP, MB and LFP interpreted the data and designed the studies with human blood; GD designed the self-renewal studies; SA and SRP performed the time lapse studies and interpreted the results; PR conceptualized the entire study, designed and interpreted the results. All authors were involved in writing the manuscript.

Additional information

Supplementary information accompanies this paper at <http://www.nature.com/scientificreports>

Competing financial interests: The authors declare no competing financial interest.

License: This work is licensed under a Creative Commons Attribution-NonCommercial-NoDerivs 3.0 Unported License. To view a copy of this license, visit <http://creativecommons.org/licenses/by-nc-nd/3.0/>

How to cite this article: Patel, S.A. *et al.* Delineation of breast cancer cell hierarchy identifies the subset responsible for dormancy. *Sci. Rep.* **2**, 906; DOI:10.1038/srep00906 (2012).